Structure, Vol. 13, 1499–1509, October, 2005, ©2005 Elsevier Ltd All rights reserved. DOI 10.1016/j.str.2005.07.005

Structural and Energetic Origins of Sequence-Specific DNA Bending: Monte Carlo Simulations of Papillomavirus E2-DNA Binding Sites

Remo Rohs,[1,3,*] Heinz Sklenar,[2,3] and Zippora Shakked[1,3]
[1]Department of Structural Biology
Weizmann Institute of Science
Rehovot 76100
Israel
[2]Max Delbrück Center for Molecular Medicine
Robert-Rössle-Str. 10
13092 Berlin
Germany

Summary

DNA bending is an important structural feature for indirect readout in protein-DNA recognition. The binding of papillomavirus E2 transcription factors to their DNA binding sites is associated with DNA bending, providing an attractive model system to study the origins of sequence-specific DNA bending. The consensus E2 target is of the general form $ACCGN_4CGGT$ with a variable four base pair region. We applied a new all-atom Monte Carlo (MC) algorithm that combines effective sampling with fast conformational equilibration. The resulting MC ensembles resemble the corresponding high-resolution crystal structures very well. Distinct bending is observed for the E2-DNA binding site with a central AATT linker in contrast to an essentially straight DNA with a central ACGT linker. Contributions of specific base pair steps to the overall bending are shown in terms of local structural parameters. The analysis of conformational substates provides new insights into the energetic origins of intrinsic DNA bending.

Introduction

DNA bending has been shown to play a major role in protein-DNA recognition and binding. Specific protein-DNA interactions such as hydrogen bonds and van der Waals contacts (Luscombe et al., 2001) require in many cases DNA deformation (Garvie and Wolberger, 2001), which is characterized by a nonlinear course of the overall helical axis. This indirect readout effect associated with DNA bending was reported for several protein-DNA complexes (Dickerson, 1998). Among them are complexes where the bends range from localized sharp kinks, as seen in DNA targets bound to the catabolite activator protein (Parkinson et al., 1996), the Lac operator (Lewis et al., 1996), and the TATA binding protein-DNA complex (Kim et al., 1993), to smooth curvature over a stretch of several adjacent base pairs, as reported for the MATa1/α2 homeodomain-DNA complex (Li et al., 1995) and the E2-DNA complexes from papillomaviruses (Hegde et al., 1992; Kim et al., 2000).

The E2-DNA system provides an attractive model system for studying indirect readout effects because DNA binding affinity of the E2 proteins depends on the identity of the DNA linker that is not involved in direct readout (Hines et al., 1998). Crystal structures of different E2-DNA targets are available in both their free and protein-bound states. The E2 proteins bind to DNA as dimers, providing two recognition α helices that form specific protein-DNA contacts with the conserved bases ACC/GGT of the 12 base pair binding site, $ACCGN_4$ CGGT. These direct readout interactions comprise both hydrogen bonds and van der Waals contacts but require a significant DNA bending. The available crystal structures of E2 proteins bound to DNA, one with the E2 protein from the bovine papillomavirus (BPV; Hegde et al., 1992) and the other with the E2 protein from the cancer-associated human papillomavirus (HPV; Kim et al., 2000), show similar overall DNA conformations (Hegde, 2002). Both complexes display smooth DNA bending or continuous curvature. The four central base pairs of the DNA binding site are not involved in protein-DNA contacts but provide the main contribution to the overall bending toward the central minor groove. In the case of DNA binding to HPV E2 proteins, AT-rich linkers replace the general sequence linker of the bovine BPV E2-DNA complexes, resulting in higher binding affinities (Hines et al., 1998).

The free DNA target of the BPV E2 protein containing an ACGT linker shows an essentially straight helix (Rozenberg et al., 1998), whereas the free DNA target of the HPV E2 protein containing the AATT linker is significantly bent toward the minor groove (Hizver et al., 2001). DNA bending by adenine-thymine tracts has been studied (Shatzky-Schwartz et al., 1997; Crothers and Shakked, 1999; Stefl et al., 2004) but the basic principles that determine indirect readout effects of such sequences are still not clearly understood. Obviously, interaction with the protein can induce or strengthen DNA bending but the ability to undergo bending is intrinsic to the base sequence. Furthermore, the crystal structures of the HPV E2-DNA binding site demonstrate that intrinsic DNA bending contributes to the higher binding affinity of the AATT target with respect to that of the ACGT one (Hines et al., 1998; Hizver et al., 2001; Hegde, 2002). However, experimental data derived from high-resolution crystal structures provide detailed structural information only on static conformations of E2-DNA binding sites. Gel electrophoretic phasing (Zimmerman and Maher, 2003) and cyclization kinetics measurements (Zhang et al., 2004) provide data on averaged helical parameters in solution.

State-of-the-art molecular modeling studies of DNA structure and dynamics have been based hitherto on molecular dynamics (MD) simulations (Cheatham and Kollman, 2000). MD studies have provided important insights into sequence-dependent structure and flexibility (Young and Beveridge, 1998; Sprous et al., 1999; Cheatham and Young, 2001; Djuranovic and Hartmann, 2003; Beveridge et al., 2004a) and intrinsic DNA bending (Strahs and Schlick, 2000; McConnell and Beveridge, 2001; Beveridge et al., 2004b; Dixit et al., 2004).

*Correspondence: mail@remo-rohs.de
[3]Lab address: http://www.remo-rohs.de

However, a satisfactory conformational equilibration cannot be reached even by extremely expensive calculations (McConnell and Beveridge, 2000; Ponomarev et al., 2004; Varnai and Zakrzewska, 2004). Moreover, despite the resemblance to experimentally reported bending magnitudes of DNA, MD trajectories show significant deviations of average structural parameters from experimental data. Most notably, the Helix Twist is systematically underestimated by 4°–7° in MD studies (McConnell and Beveridge, 2000, 2001; Strahs and Schlick, 2000; Cheatham and Young, 2001; Beveridge et al., 2004a). MD simulations of the HPV E2-DNA binding site (4 ns; Byun and Beveridge, 2004) and of the BPV E2-DNA target (15 ns; Djuranovic et al., 2004) reflect the concerns regarding equilibration and Helix Twist. Unlike the aforementioned MD studies of DNA in explicit water, a minimal solvation MD model (Mazur and Kamashev, 2002) improves the convergence and the Helix Twist values but results in damped conformational sampling (Cheatham and Young, 2001).

The lack of experimental atomic resolution data on the dynamics of such systems and the mentioned limitations of MD simulations led us to apply our new Monte Carlo (MC) algorithm (Rohs, 2002; Sklenar et al., 2005) on the E2-DNA binding sites. Here, we present all-atom MC simulations of DNA oligomers based on this algorithm that combines the constant bond lengths approximation and an analytical chain closure with collective variable moves. The MC algorithm ensures local moves of chain conformation and results in effective conformational sampling and fast equilibration (Rohs, 2002). The structural analysis demonstrates that the MC trajectories resemble the experimental data in terms of global and local structural features of DNA bending. The data provide further understanding of sequence-dependent DNA deformations by revealing local contributions of base pair steps to the overall bending. The analysis of the MC trajectories in energetic terms identifies specific interactions that induce and stabilize DNA bending.

Results

Equilibration of MC Simulations

Molecular modeling algorithms are suitable to generate data on structural flexibility and dynamics if the conformational sampling is efficient. This means that the majority of the conformational space is sampled and the simulations reach equilibration within a reasonable CPU time. In other words, molecular modeling results provide relevant information only if the equilibrated simulations result in an ensemble of conformations that is characterized by stabilized average properties. The equilibration of the total energy is a necessary but not a sufficient criterion for this process because similar energy values might be assigned to substates with different conformations. The results of the MC simulations of the DNA targets with ACCGAATTCGGT (referred to as MC-AATT) and ACCGACGTCGGT (referred to as MC-ACGT) sequences are presented in Figure 1. Both energetic and structural equilibration is reached, as demonstrated by the average values of the energy and the various structural parameters over the course of the simulations. The total energy reaches stable average values for the two MC runs within <0.5 million MC cycles. Accumulated averages of structural properties, shown in Figure 1, reflect the more rigorous criterion of structural equilibration. The average rms deviation of MC snapshots equilibrates within 0.75 million MC cycles for the MC-AATT and MC-ACGT simulation. The average values of individual helical inter-base pair parameters, Roll and Helix Twist, over the course of the MC-AATT simulation illustrate equilibration of local structural properties. Equilibration of such parameters is also reached within 0.75 million MC cycles, and the corresponding average values show a sequence-dependent behavior that reflects the palindromic symmetry of the sequence, thus providing further evidence for equilibration.

Structural Analysis and Comparison with Crystal Structures

The structural characterization of the MC simulations is performed in terms of global and local parameters focusing on local DNA deformations that lead to global DNA bending. Average values of structural parameters are calculated for the equilibrated part of the MC simulations between 0.75 and 2.25 million MC cycles. Consistently, each tenth MC snapshot of the equilibrated MC trajectory is used for the structural analysis, generating averages on the basis of 150,000 conformations. Standard deviations of structural parameters, denoted as fluctuations, are calculated accordingly.

First, we calculated rms deviations between MC snapshot conformations and the crystal structures in the free and protein-bound states. Rms deviations for the DNA targets comprising 24 nucleotides, derived from least square fitting of all heavy-atom Cartesian coordinates, are given in Table 1. Average rms deviations close to 2 Å with standard deviations of 0.4 Å reflect considerable resemblance of the MC ensembles MC-AATT and MC-ACGT with the corresponding high-resolution crystal structures of the free DNA, placing the MC ensembles well within the B-DNA family. Superimposing four base pair tracts of the MC-AATT simulation onto the crystal structures results in average rms deviations between 1.2 Å and 1.7 Å for the ACCG and CGGT tracts at each end of the AATT dodecamer and only 0.8 Å for the central AATT linker. This difference in rms deviations reflects higher flexibility of the end base pair tracts compared to the relatively rigid central region. For the second sequence, corresponding comparisons result in similar average rms deviations ranging from 1.2 Å to 1.7 Å for all three regions ACCG, ACGT, and CGGT, indicating that the ACGT linker can undergo larger conformational rearrangements upon protein binding than the stiffer AATT linker.

It should be noted that the crystal structures X1 to X3-AATT of the free AATT dodecamer were shown to be significantly bent toward the minor groove (Hizver et al., 2001), whereas X1 to X4-ACGT of the free ACGT dodecamer were essentially straight (Rozenberg et al., 1998), although binding to the E2 protein requires considerable bending toward the minor groove of the central linker. Low rms deviations between MC ensembles and the free DNA crystal structures also indicate

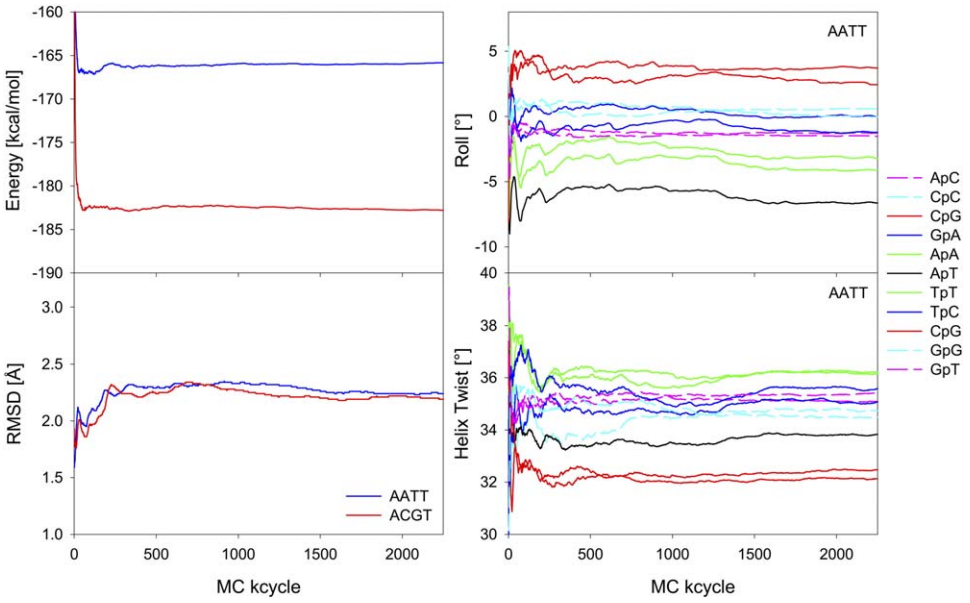

Figure 1. Accumulated Averages of Energy Values and Structural Parameters over the Course of the MC Simulations

Total energy of the MC-AATT and MC-ACGT system, rms deviations with respect to the crystal structures X1-AATT and X1-ACGT (left panel), and Roll and Helix Twist values of the individual base pair steps for the MC-AATT system (right panel) are shown as functions of MC cycles. Stable average values prove that energetic and structural equilibration is reached after 0.75 million MC cycles. Note that the helical parameters after equilibration reflect the palindromic symmetry of the base sequence.

that MC simulations reflect the intrinsic bending of the free DNA. This hypothesis is further tested by calculating average rms deviations of the MC ensembles and the protein-bound DNA molecules, XC-AATT bound to the HPV E2 protein (Kim et al., 2000) and XC-ACGT bound to the BPV E2 protein (Hegde et al., 1992), which are both more deformed and bent than any of the free DNA dodecamers. Interestingly, the corresponding rms deviations differ significantly with 2.9 Å for MC-AATT, with respect to XC-AATT, and 4.3 Å for MC-ACGT, with respect to XC-ACGT, whereas the corresponding values with respect to the free DNA crystal structures were similar (Table 1). This finding further proves that the MC-AATT ensemble snapshots adopt on average a conformation that is more similar to the protein-bound form in comparison with that of the MC-ACGT ensemble.

Schematic representations of the two dodecamer ensemble averages with their global helix axes, based on the equilibrated range of the MC simulations, are shown in Figure 2 (generated by the CURVES algorithm (Lavery and Sklenar, 1988, 1989). DNA bending can be characterized by a nonlinear course of the global helix axis and the corresponding effects on the geometry of the grooves. The average structure of the MC-AATT ensemble is bent toward the minor groove as shown by the direction of the helix axis in Figure 2A. In comparison, the global helix axis of the MC-ACGT ensemble shown in Figure 2C is straight. The distinct bending of the MC-AATT average structure is associated with a narrowing of the minor groove relative to that of the MC-ACGT average conformation, illustrated in Figures 2B and 2D.

The effect of DNA bending on the minor groove geometry is shown in Figure 3 by plotting the changes in the width and depth of the minor groove along the DNA sequence for both the MC and X-ray data. The minor groove width of the bent MC-AATT conformation is

Table 1. Average Rms Deviations between MC Snapshot Conformations and the Corresponding Crystal Structures

AATT linker		ACGT linker	
Crystal structure	MC rmsd (Å)	Crystal structure	MC rmsd (Å)
X1-AATT	2.2 ± 0.4	X1-ACGT	2.1 ± 0.4
X2-AATT	2.1 ± 0.4	X2-ACGT	2.2 ± 0.4
X3-AATT	2.3 ± 0.4	X3-ACGT	2.2 ± 0.4
		X4-ACGT	2.1 ± 0.4
XC-AATT	2.9 ± 0.5	XC-ACGT	4.3 ± 0.6

The rms calculations are based on heavy atoms of DNA dodecamers of every tenth MC cycle after equilibration. Note that the average rms deviations between the MC ensemble and the crystal structures of the free DNA are very reasonable, whereas the rms deviations are slightly larger with respect to the complex XC-AATT and much larger with respect to the complex XC-ACGT.

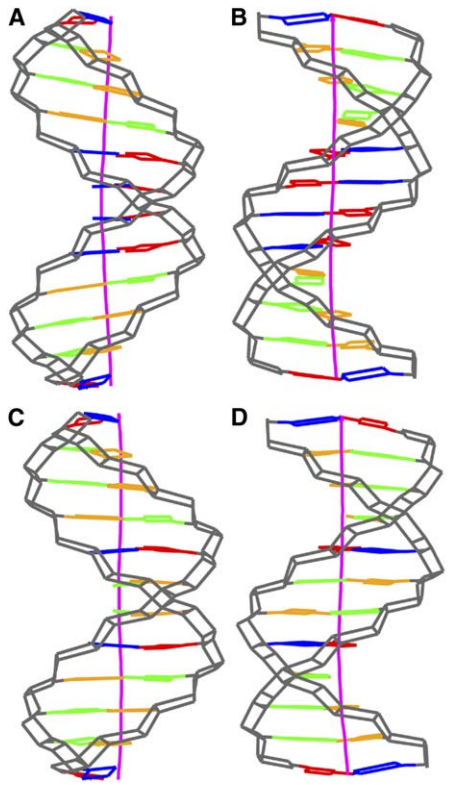

Figure 2. Average Conformations of the Equilibrated Ensembles

Schematic representations include global helical axes calculated by CURVES ([A and B] MC-AATT; [C and D] MC-ACGT). The structures are based on the snapshots of every tenth MC cycle after equilibration. The views shown for each sequence are both perpendicular to the helical axis, either toward the phosphodiester backbone (A and C) or into the minor groove (B and D). The different bases can be distinguished by colors (adenine, red; thymine, blue; guanine, green; cytosine, yellow) complemented by the phosphodiester backbone (in black) and the helical axes (in magenta). Note the global helical axis bending (A) and minor groove narrowing (B) of the MC-AATT in comparison with the MC-ACGT average structure (C and D).

characterized by a dramatic narrowing at the center (3.6 Å) that is in excellent agreement with the average values of the crystal structures (Hizver et al., 2001). Groove narrowing is usually associated with groove deepening as shown here as well. The minor groove depth reaches its maximum value (4.8 Å) at the center, again in excellent agreement with the corresponding average value of the X-ray structures (4.9 Å). In general, the minor groove width and depth patterns are similar between the MC ensemble averages and the crystal structures. However, deviations between the simulated and the experimental conformations are displayed by the minor groove width of the ACGT helix. This observation may be related to the large variance in the minor groove width of the crystal structures (Rozenberg et al., 1998). X1 and X4-ACGT show wide minor grooves (up to 7.2 Å), and X2 and X3-ACGT show significantly narrower minor grooves with the X3-ACGT minor groove width of 4.8 Å at the center being in perfect agreement with the MC-ACGT average, as shown in Figure 3.

Local structural deformations and contributions toward overall bending are analyzed in terms of helical parameters. Roll, Tilt, and Helix Twist characterize rotations between adjacent base pairs. The major contribution toward bending arises from Roll because a positive Roll compresses the major groove and a negative Roll compresses the minor groove. As shown in Figure 4, the two CpG base pair steps of the MC-AATT structures show average Roll values between 2.3° and 3.7° in a direction that compresses the major groove. The central ApT base pair step displays a negative average Roll of –7.2° compressing the minor groove and hence contributing to compression or bending toward the minor groove. The crystal structures X1 to X3-AATT show symmetrized average Roll values of 4.3° for the CpG steps and –2.5° for the ApT step in agreement with the Roll pattern seen in the MC data. The central ApT base pair step is replaced by a CpG base pair step in the MC-ACGT sequence, resulting in three CpG base pair steps with positive Roll values between 3.0° and 4.6° as shown in Figure 4, both in agreement with the crystal structures of X1 to X4-ACGT whose symmetrized averages are 5.0° for the peripheral CpG steps and 6.9° for the central CpG step. The positive Roll of the central CpG base pair step partly counteracts the bending caused by the two peripheral CpG base pair steps as they are three base pairs apart, resulting in an essentially straight helix. In contrast, the AATT helix displays a pronounced intrinsic bending due to the combined effects of the positive Roll at the CpG doublets and the negative one at the central ApT step.

Tilt contributes further toward bending but to a lesser degree due to steric effects with the sugar-phosphate backbone, and hence the sequence-dependent variations of Tilt are small. The average Tilt values of –1.6° for the ApA and 1.6° for the TpT base pair step reinforce the bending of the MC-AATT structure in good agreement with the X-ray structures with values of –2.4° for the ApA step and 2.4° for the TpT step on the basis of symmetrized averages of X1 to X3-AATT. Much smaller average Tilt values between –0.3° and 0.3° of the central region of the MC-ACGT ensemble are in accordance with its straighter average conformation.

The Helix Twist characterizes inter-base pair rotations with respect to the helical axis. DNA bending is associated with deviations of the Helix Twist from standard B-DNA values. For example, significant positive or negative Roll values may be associated with untwisting or overtwisting of respective base pair steps depending on the identity of the base pair doublet (Olson et al., 1998). The positive Roll values of the peripheral CpG steps are correlated with lowered average Helix Twists between 32.1° and 32.6° for both sequences, whereas the central CpG step displays a significantly higher Helix Twist, as shown in Figure 4. The negative Roll at the center of the MC-AATT structure is associated with an average Helix Twist of 34.0°, whereas the smaller negative Roll angles of the neighboring steps show larger Helix Twists of up to 36.5°. This pattern is similar to the one shown by the crystal structures of X1 to X3-AATT. The Helix Twist pattern of MC structures with the ACGT linker also resembles that of the crystal structures (X1 to X4-ACGT). Although the general shape of the Helix Twist pattern derived from X-ray data is conserved, the

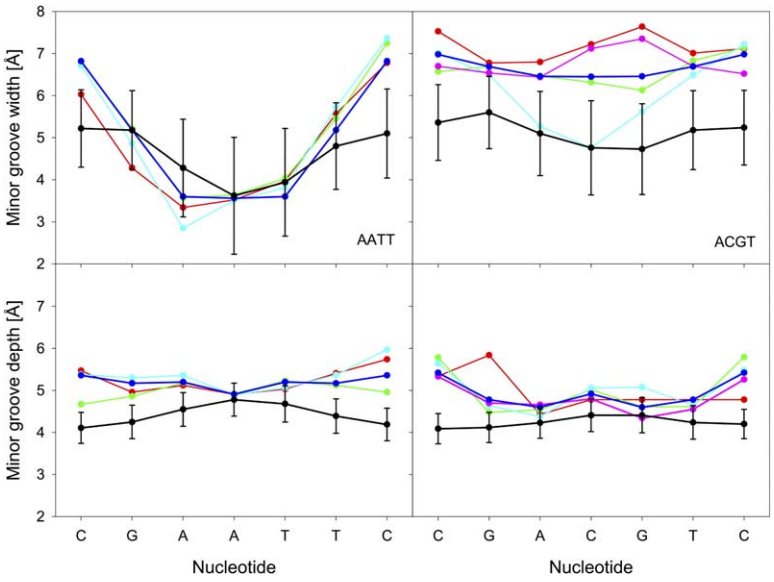

Figure 3. Minor Groove Width and Depth as Functions of the Base Sequences

The MC average values (in black) are based on the structures of every tenth MC cycle after equilibration. Fluctuations are shown as error bars. High-resolution X-ray data are shown for comparison (AATT: X1 in red, X2 in green, X3 in cyan; ACGT: X1 in red, X2 in green, X3 in cyan, X4 in magenta). The X-ray structural data were averaged and symmetrized (shown in blue).

large differences in the values of the central ACGT linker are damped in the MC data.

High Propeller Twist values were shown to be a characteristic feature of A-tract DNA (Crothers and Shakked, 1999). Figure 4 illustrates that the structures of MC-AATT and MC-ACGT differ significantly by the Propeller Twist values of their central regions. The AATT linker shows average Propeller Twist values between –10.2° and –11.4° for the four consecutive base pairs in comparison with lower values between –7.5° and –8.3° for the ACGT linker. In accordance with the crystal structures, the MC data of both sequences show negative Propeller Twists in these regions with lower values for the AATT linker than for other regions. The Propeller Twist was discussed in former studies in relation to sugar puckering (Strahs and Schlick, 2000). The sugar phases occupy mainly C2′-endo conformations with short-living excursions toward C3′-endo and O1′-endo states. However, the average phase angles of purine nucleosides are larger than those of pyrimidine nucleosides with values of 155° for adenosines, 148° for thymidines, 155° for guanosines, and 144° for cytidines.

Next, we examined the relationship between DNA bending as reflected by minor groove compression and local helical parameters. The minor groove width at the center of the structures is shown in Figure 5 as a function of either Roll or Helix Twist averaged over the three base pair steps of the central linker regions. The correlation coefficients relating minor groove width with Roll are 0.81 for AATT and 0.69 for ACGT, and the corresponding numbers for the Helix Twist are –0.50 for AATT and –0.46 for ACGT. The MC data prove that the local inter-base pair geometry determines DNA bending and that bending is more correlated with Roll than with Helix Twist. In addition, these correlations are stronger for the MC-AATT than for the MC-ACGT ensemble, reflecting the larger intrinsic bending of the DNA target with AATT linker. Bending toward the minor groove is represented by minor groove compression, which is achieved, at least in part, by a negative Roll in conjunction with an increased Helix Twist.

The global bend angle is 10° for the MC-AATT ensemble average (in comparison with 8°, 11°, and 8° for X1 to X3-AATT) unlike the essentially straight nature of the MC-ACGT sequence, both in accordance with the crystal structures. The helix axes and minor grooves of the corresponding average structures in Figure 2 illustrate the pronounced bending of the MC-AATT ensemble in comparison with the MC-ACGT ensemble. It should be noted from Figure 3 that the individual crystal structures with the ACGT linker are characterized by either minor groove narrowing or widening in contrast to the directed bending of the DNA targets with the AATT linker.

Local bend angles between consecutive base pairs were calculated. The local bend angle pattern as a function of base pair steps is shown in Figure 6 for the MC ensembles and X-ray structures. Most significantly, the local bend angles of CpG base pair steps are elevated in comparison with the neighboring base pair steps, forming peaks ranging between 4.8° and 5.5° for both the MC-AATT and the MC-ACGT structures. This bend angle pattern is conserved for the averaged values of the crystal structures although the latter are shifted by 1°–2° toward smaller values.

Energetic Origins of Intrinsic DNA Bending

The driving forces of intrinsic bending are of considerable interest for understanding the physical principles of DNA bending. For this reason, a representative bending event within the trajectory of the MC-AATT trajectory has been chosen by the criterion that it describes a typical excursion from a straight helix toward significantly bent DNA and backward. This bending event between the 600,000th and 700,000th MC cycle is structurally characterized by the minor groove width shown in Figure 7. Relative changes of critical energy contributions upon this bending event presented by minor groove narrowing are shown in Figure 7 as energy differences for MC snapshots along the trajectory.

The chosen bending event is characterized by a dra-

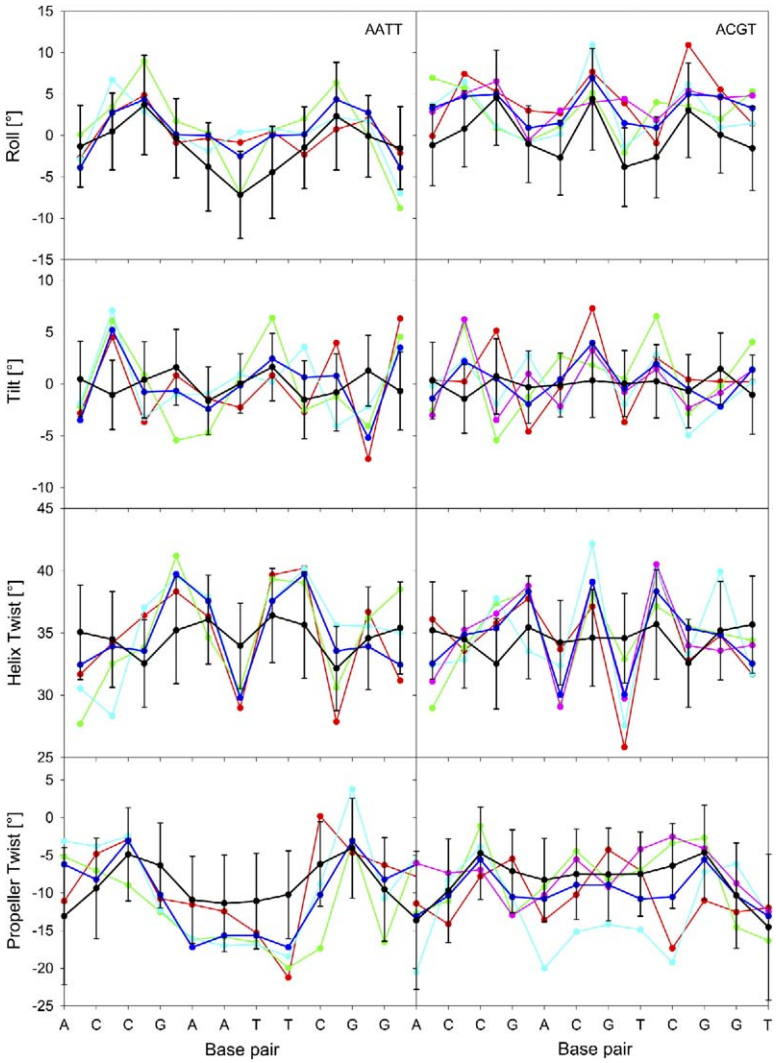

Figure 4. Helical Parameters Roll, Tilt, Helix Twist, and Propeller Twist as Functions of the Base Sequences

The MC average values (in black) are based on the structures of every tenth MC cycle after equilibration. Fluctuations are shown as error bars. X-ray structural data are shown for comparison including their symmetrized averages (color code as in Figure 3). Note the well-preserved symmetry of the MC data reflecting the palindromic nature of both sequences.

matic narrowing of the central minor groove from around 6 Å to 2 Å within the first 20 MC kcycles followed by 40 MC kcycles with a narrow minor groove. After 60 MC kcycles, the central minor groove widens up to around 4 Å, closes again gradually after 80 MC kcycles, and opens up after completing the excursion of 100 MC kcycles, finally reaching its original width of approximately 6 Å. It should be pointed out that MC trajectories do not allow conclusions on the timescale of dynamical behavior. However, the structural and energetic interplay of local conformational changes required to achieve global transitions between substates is well reflected by MC data.

What are the driving forces for such bending events and what are the energy contributions that stabilize bent DNA conformations? Both van der Waals energy contributions of backbone-backbone and backbone-base interactions become more favorable over the initial 20 MC kcycles of minor groove narrowing. The data suggest that the specified van der Waals interactions act as the driving forces of intrinsic bending. van der Waals backbone-backbone interactions become more favorable due to the closing of the minor groove. van der Waals backbone-base interactions are characterized by rearrangements of the bases with respect to the backbone. Conformational changes in this bending process include the overtwisting of specific base pairs, excursions of individual sugar moieties within the bending scope toward the C1′-exo sugar puckering mode in conjunction with moderate changes in the glycosidic angles. After reaching the narrow minor groove conformation, the electrostatic energy contributions of backbone-base and counterion-DNA interactions stabilize the bent conformation, together with the van der Waals energy contributions of both backbone-backbone and backbone-base interactions. In contrast to the above interactions, the energy contributions of electrostatic backbone-backbone and van der Waals base-base interactions as well as the deformation energy of torsion and bond angles gradually disfavor the bending over the course of the initial 40 MC kcycles. Whereas van der Waals backbone-backbone interactions become favorable in the course of bending, electrostatic backbone-backbone interactions oppose

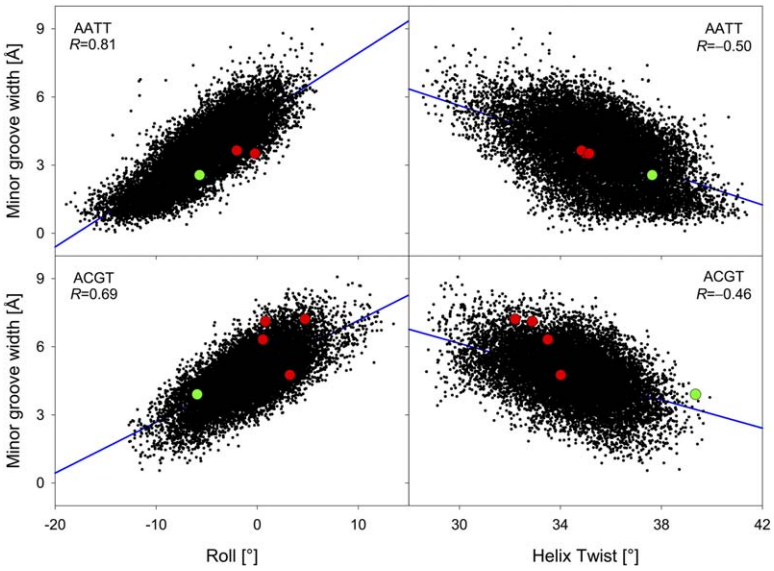

Figure 5. Correlations of the Minor Groove Width in the Central Linker Region and the Helical Parameters Roll and Helix Twist

The helical parameters are averaged over the four base pair linker. The values are based on snapshot conformations of every 100th MC cycle after equilibration (in black). The linear regression line for the MC ensemble structures (in blue) and the data for the crystal structures of the free DNA (in red) and the DNA in the respective complexes (in green) are included as well as the corresponding correlation coefficients *R*.

bending because the highly charged phosphate groups of opposite strands become closer upon minor groove narrowing.

The energy contributions that stabilize bent conformations are altered in the second stage of the bending excursion (after the initial 40 MC kcycles). As shown in Figure 7, the deformation energy of torsion and bond angles, the van der Waals energy of base-base interactions, and the electrostatic energy of backbone-backbone interactions contribute gradually to a further stabilization of the bent DNA conformation (over the course of the following 40 MC kcycles). After the larger backbone deformations as a result of bending, backbone relaxations cause more favorable contributions of the torsion and bond angle deformation energy. The sugar moieties and backbone torsion angles within the bending scope adopt conformations which are well within the range of standard B-DNA values. Moreover, the base-stacking geometry results in more favorable base-base van der Waals interactions, most notably by reversing the unwinding of the central base pair steps. The electrostatic energy of backbone-backbone interactions contributes also toward the stabilization of bending but acts in a "tug-of-war" manner with the van der Waals backbone-backbone interactions. The more favorable electrostatic interactions between the heterocyclic bases are in contrast to the less favorable van der Waals interactions between the bases, unlike the opposite trend during the initial stage of bending. Finally, the increasingly unfavorable van der Waals backbone-backbone interaction is joined by a gradually increasing unfavorable van der Waals backbone-base interaction. This cooperative effect ends the bending excursion after 100 MC kcycles, leading to essentially straight DNA conformations.

Discussion

Structural Features of Intrinsic DNA Bending

The MC simulations result in structural averages that are in accordance with the crystal structures of the free DNA binding sites (Rozenberg et al., 1998; Hizver et al., 2001). The typical pattern of large positive Roll values in correlation with low Helix Twist values of pyrimidine-purine steps leading to major groove compression (Gorin et al., 1995; Olson et al., 1998) is observed for all CpG base pair steps. The tendency of pyrimidine-purine steps to undergo local bends has been attributed to the reduced overlap between the adjacent base pairs (Olson et al., 1998). The tendency of certain purine-pyrimidine steps to compress the minor groove via negative Roll angles (Dickerson, 1998) is observed for the ApT base

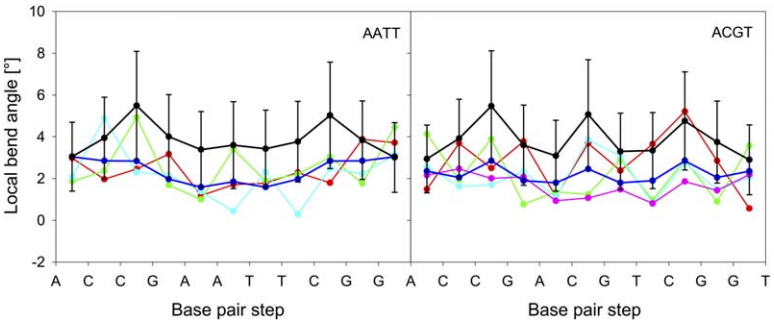

Figure 6. Local Inter-Base Pair Bend Angles as Functions of the Base Sequences

The MC average values (in black) are based on the structures of every tenth MC cycle after equilibration. Fluctuations are shown as error bars. X-ray structural data are shown for comparison including their symmetrized averages (color code as in Figure 3).

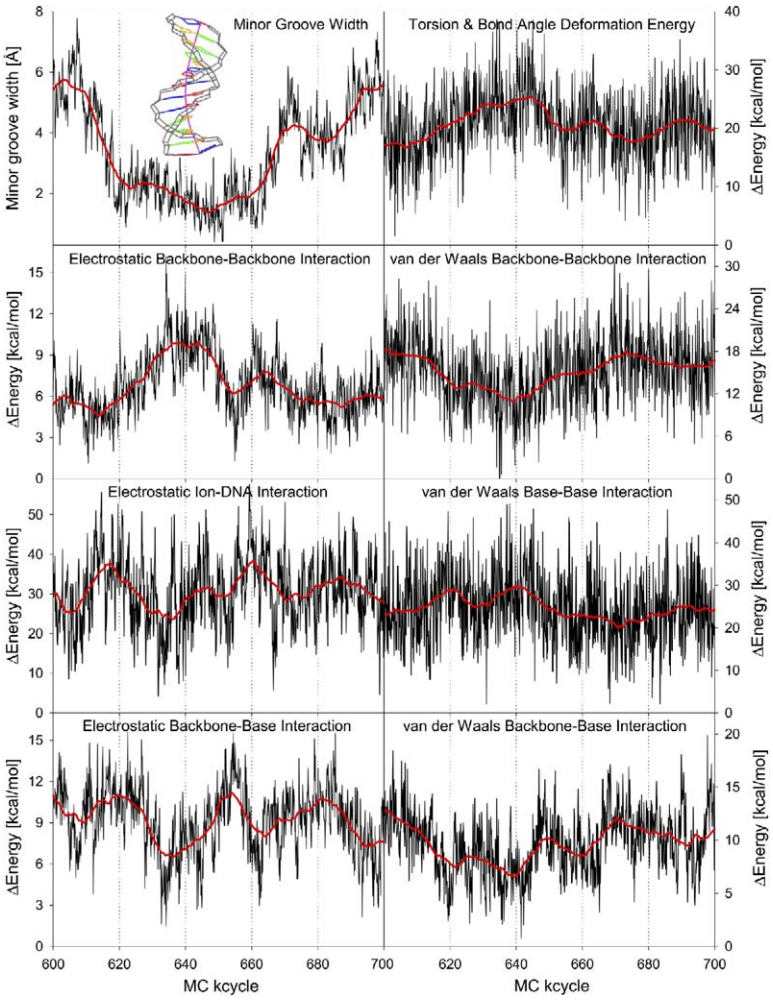

Figure 7. Minor Groove Width and Energy Components for a Bending Excursion as Functions of MC Cycles

The AATT trajectory shows a representative bending event between the 600,000th and 700,000th MC cycles. The DNA bending is characterized by the minor groove width and the corresponding energy contributions given as relative energy differences. MC snapshot values of every 100th MC cycle (in black) are complemented by their smoothed course over the MC trajectory (in red). The upper left panel shows a CURVES-generated schematic representation of the average structure during the bending excursion between the 620,000th and 660,000th MC cycles. The electrostatic base-base interaction, the van der Waals ion-DNA interaction, and the ion-ion interaction energy are not shown due to their nonsignificant altering upon bending.

pair step of the AATT linker. The different behavior of CpG and ApT steps has been explained in terms of clashes between amino groups in the minor groove of CpG steps and in the major groove of ApT steps (Gorin et al., 1995). In a similar manner to the crystal structures, the curvature of the MC-AATT versus the MC-ACGT ensemble is generated mainly by the distribution of CpG and ApT steps along the base sequence. Two CpG steps separated by six base pairs and the central ApT step compress the major and minor groove of the MC-AATT target toward the same general direction, resulting in overall bending. In contrast, the central CpG step of the MC-ACGT sequence opposes the bending caused by the peripheral CpG steps.

X-ray crystallography and NMR spectroscopy studies show that short runs of adenine-thymine base pairs known as A-tracts are intrinsically bent (Shatzky-Schwartz et al., 1997; Stefl et al., 2004). The contribution of ApT base pair steps to A-tract bending is associated with negative Roll that compresses the minor groove (Crothers and Shakked, 1999). Solution studies of the E2-DNA binding sites further confirm the bending of DNA targets with AATT linker versus no significant curvature of DNA targets with ACGT linker (Zimmerman and Maher, 2003; Zhang et al., 2004). The presented MC data corroborate a bending model characterized by minor groove narrowing in A-tracts in conjunction with major groove compression in the adjacent non-A-tract regions (Crothers and Shakked, 1999).

Equilibration as a Criterion for the Relevance of Simulation Results

Fast equilibration of the applied MC methodology is demonstrated in terms of energy, rms deviations, and helical parameters. In contrast, MD bending studies with the utmost 15 ns trajectories do not provide evidence of equilibration (Strahs and Schlick, 2000; McConnell and Beveridge, 2001; Byun and Beveridge, 2004; Djuranovic et al., 2004). MD studies of small DNA molecules sample only a minor fraction of the conformational space even in 50 ns simulations (Cheatham and Young, 2001). Long-lasting conformational substates were reported by a 15 ns MD study suggesting that backbone transitions prevent a complete conformational sampling for B-DNA in such simulations (Beveridge et al., 2004a). In another study, ions were extrapolated to converge reasonably within 100 ns MD simulations (Beveridge et al., 2004b) on the basis of a 60 ns MD run that required about 6 months of computational time (Ponomarev et al., 2004). In a related work,

the fraction of available space visited by an individual ion in a 50 ns MD run was around 30%–40% (Varnai and Zakrzewska, 2004). The same MD study reports on noncanonical DNA backbone conformations that occur after 20 ns.

A Comparison between MC and MD Simulations

The 4 ns MD study of the HPV E2-DNA binding site reports on average rms deviations from the crystal structures of 2.7–3.0 Å (Byun and Beveridge, 2004) in comparison with the current MC result of 2.1–2.3 Å. The minor groove narrowing of the MC ensemble with an average minor groove width in the central region of 3.6 Å is in agreement with the experimental values of 3.5–3.6 Å unlike the ~5 Å value of the MD simulations. The global DNA bending of 16° observed in the MD simulations is mainly due to localized kinks at the two CpG steps. The MC global bend angle of 10°, which is in better accordance with experimental data, is caused mainly by positive Roll values of the CpG steps and a negative Roll of the central ApT step. In addition, the average Tilt values in the MC simulations resemble closely the characteristics of the crystal structures in contrast to the MD data with positive Tilt values of both the ApA and the TpT step, these being also in contradiction to the symmetry of the molecule. The Helix Twist is probably the most controversial issue between the two methods. The MC data correspond reasonably well with both the magnitude and sequence effects of the Helix Twist, whereas the MD data result in a dramatic helix unwinding with average Helix Twist values of 23°–27° for CpG steps (Byun and Beveridge, 2004). This systematic unwinding was attributed to the Cornell et al. (1996) AMBER force field (Byun and Beveridge, 2004). However, the same force field does not lead to unwinding in the present MC simulations.

The 15 ns MD study of BPV E2-DNA binding sites claims an effective conformational sampling because different MD runs result in average structures that differ by an rms deviation of only 0.7 Å (Djuranovic et al., 2004). In comparison, the ensemble average structures for the MC runs starting from canonical B-DNA and from the crystal structures result in an rms deviation of <0.4 Å. The Roll pattern with its maxima at the CpG base pair steps is similar for the MC and MD data. However, the MD simulations significantly underestimate the Helix Twist with average values of ~23°–25° for the peripheral CpG steps and ~27°–28° for the ApC and the GpT steps (Djuranovic et al., 2004) in contrast to the MC values.

Two 15 ns MD studies of ACGT tracts in different base sequence contexts with controversial results were recently performed (Beveridge et al., 2004a; Djuranovic et al., 2004). One study reports on frequent BI/BII transitions suggesting their relevance for DNA bending (Djuranovic et al., 2004), and the other one discusses long-living α/γ flips stating that slow backbone transitions prevent a complete MD sampling (Beveridge et al., 2004a). Our previous MC simulations ascertained that the Cornell et al. AMBER force field (Cornell et al., 1996) favors BII over BI conformations, resulting in transitions of all nucleotides to the noncanonical BII conformation associated with dramatic overtwisting resembling D-DNA within an early phase of equilibration (Rohs, 2002). We concluded that this tendency to favor helix overwinding associated with BII backbone conformations is due to a force field artifact that affects MC simulations as they easily cross high barriers and reach unrealistic local minima.

We agree with other research groups that the thorough understanding of DNA dynamics should include the description of short-lived noncanonical backbone conformations (Winger et al., 1999; Djuranovic and Hartmann, 2003). However, our findings confirm the conclusion of a recent 15 ns MD study that the conformational backbone sampling is unsatisfactory with nowadays' force fields (Beveridge et al., 2004a). To overcome this shortcoming, we introduced an energy term that stabilizes BI relative to BII conformations (see Experimental Procedures). As a result, the MC simulations of the PV E2-DNA binding sites sample the backbone conformations including BI/BII transitions and α/γ flips, whereas the majority is of canonical backbone conformations. However, the resemblance of bending-related structural parameters and global bending of the MC ensemble averages with that of the crystal structures (Rozenberg et al., 1998; Hizver et al., 2001) suggests that noncanonical backbone conformations are not essential for DNA bending. Based on our results that propose conformational origins of intrinsic DNA bending, we believe that BII conformations are induced by bending-related DNA deformations rather than the other way around.

Conclusions

We applied a new all-atom MC algorithm to investigate the intrinsic DNA bending of papillomavirus E2-DNA binding sites. The MC simulations of the two DNA targets with AATT and ACGT central linkers demonstrate fast equilibration and efficient sampling of the conformational space. Global and local features of the intrinsic DNA bending resemble very well those obtained by high-resolution crystal structures. Average rms deviations between MC ensembles and the crystal structures indicate that the flexibility of the PV E2 binding sites is dependent on the identity of the central linker sequence, with AATT being more rigid than ACGT or the peripheral ACCG/CGGT tracts. The stronger intrinsic bending of the MC-AATT versus the MC-ACGT sequence is in accordance with X-ray data. Several helical parameters (Roll, Tilt, Helix Twist, and Propeller Twist) that are associated with DNA bending were analyzed. Both the CpG and ApT base pair steps show local bending leading to global bending. The MC simulations also yield information on the flexibility of DNA bending in terms of fluctuations in the bending-related parameters, thus providing further insights into sequence-dependent bending and flexibility and their effects on protein-DNA recognition.

The energetic analysis classifies the various types of interactions regarding their role contributing to intrinsic DNA bending. van der Waals backbone-base and backbone-backbone interactions are the driving forces of intrinsic bending, whereas electrostatic backbone-base and counterion-DNA interactions act as stabilizing forces at the initial state of bending. After the initial stage,

DNA bending induces structural rearrangements of mainly base-stacking and torsion angle geometry. The bending in this stage is stabilized by energy contributions of torsion and bond angle deformations, van der Waals base-base interactions, and electrostatic backbone-backbone interactions. Concurrently, the initially stabilizing van der Waals backbone-backbone and backbone-base interactions gradually oppose intrinsic DNA bending, and finally reverse it to straight DNA. Thus, interactions that initially induce bending and those that stabilize bent conformations are of different origins. The "tug-of-war" between them determines the flexibility and the intrinsic DNA bending characteristics of various E2-DNA binding sites.

Experimental Procedures

All-atom Monte Carlo simulations (Rohs, 2002) of the DNA binding sites 5′-ACCGAATTCGGT-3′ and 5′-ACCGACGTCGGT-3′ were performed over 2.25 million MC cycles starting from canonical B-DNA conformation. MC simulations with identical protocols were also performed with the crystal structures as initial conformations. MC ensemble averages and fluctuations were calculated for equilibrated MC trajectories of 1.5 million MC cycles following the initial 0.75 million MC cycles. Because all-atom rms deviations between average structures started from either canonical B-DNA or the crystal structures are <0.4 Å, the MC simulations are largely independent of their starting configurations. Therefore, only trajectories starting from canonical B-DNA are discussed in detail. The MC trajectories of the DNA targets differing by their central linker sequences (AATT and ACGT) are denoted as MC-AATT and MC-ACGT.

Our new MC algorithm is based on the assumption of rigid bases and fixed bond lengths that enables a definition of MC moves in the space of collective and internal variables (Rohs, 2002). The set of 12 MC variables per nucleotide is composed of six collective variables (three rigid body translations and three rigid body rotations) and six internal variables (phase and amplitude of the sugar moiety following the pseudorotation description of sugar puckering [Altona and Sundaralingam, 1972; Gabb et al., 1995], the glycosidic angle, and two selected endocyclic dihedrals complemented by one endocyclic bond angle). The MC moves of these variables are combined with an analytical chain closure algorithm defined in the bond/torsion angle space (Sklenar et al., 2005), which varies the other endocyclic backbone torsion and bond angles as dependent variables. The molecular model ensures local MC moves restricted to single nucleotides and allows for an efficient conformational MC sampling (Rohs, 2002). The MC acceptance criterion follows the Metropolis algorithm (Metropolis et al., 1953) and includes associated Jacobians (Sklenar et al., 2005). The polyanionic DNA is neutralized by sodium counterions, which are moved by additional MC variables describing ion translations. Varying the defined 12 MC variables for each nucleotide in conjunction with the respective chain closures and three orthogonal MC translation moves of each of the counterions completes an MC cycle (Rohs, 2002).

Former MC approaches for DNA were either based on nonlocal moves that impeded sufficient sampling (Gabb et al., 1997) or were limited to interactions of adjacent nucleotides and neutralized phosphates (Zhurkin et al., 1991). It should be emphasized that our chain closure algorithm is a purely analytical approach in the torsion and valence angle space, unlike numeric chain closure methods defined only in the torsion angle space, which also restrict the conformational sampling (Zhurkin et al., 1991).

The Cornell et al. AMBER force field (Cornell et al., 1996) and an implicit electrostatic solvent description (Hingerty et al., 1985) are used for energy calculations. We think that the simplified model of a distant-dependent electrostatic damping used here (Rohs et al., 1999) is justified because it generates MC results which are in very good agreement with experimental data, without the computationally expensive explicit solvent. Another advantage of MC simulations in implicit solvent is that the counterions equilibrate rapidly and lose their individuality already after 10^5 MC cycles. All sodium ions sample the whole space represented by a cylinder with a radius of 100 Å around the global helix axis including frequent ion intrusions into both grooves. The energy minimum of the noncanonical BII conformation of the ϵ and ζ torsion angles was increased relative to the energy minimum of the canonical BI conformation by adding a harmonic energy term (Rohs, 2002), which has no influence on the common B-DNA BI conformation. It is also complemented by a harmonic energy term favoring the *trans* conformation of the β torsion angle (Rohs, 2002). The calculation of helical parameters and groove geometry is based on the CURVES algorithm (Lavery and Sklenar, 1988, 1989; Stofer and Lavery, 1994).

Acknowledgments

We thank Professor Barry Honig for his constant interest, encouragement, and critical comments on the manuscript. R.R. acknowledges the Minerva Foundation (Max Planck Society for the Advancement of Science) for funding by a Minerva postdoctoral fellowship. Z.S. acknowledges support from the Israel Science Foundation and the Helena Rubinstein professorial chair in structural biology.

Received: May 2, 2005
Revised: July 14, 2005
Accepted: July 14, 2005
Published: October 12, 2005

References

Altona, C., and Sundaralingam, M. (1972). Conformational analysis of the sugar ring in nucleosides and nucleotides. A new description using the concept of pseudorotation. J. Am. Chem. Soc. *94*, 8205–8212.

Beveridge, D.L., Barreiro, G., Byun, K.S., Case, D.A., Cheatham, T.E., III, Dixit, S.B., Giudice, E., Lankas, F., Lavery, R., Maddocks, J.H., et al. (2004a). Molecular dynamics simulations of 136 unique tetranucleotide sequences of DNA oligonucleotides. I. Research design and results on d(C_pG) steps. Biophys. J. *87*, 3799–3813.

Beveridge, D.L., Dixit, S.B., Barreiro, G., and Thayer, K.M. (2004b). Molecular dynamics simulations of DNA curvature and flexibility: helix phasing and premelting. Biopolymers *73*, 380–403.

Byun, K.S., and Beveridge, D.L. (2004). Molecular dynamics simulations of papilloma virus E2 DNA sequences: dynamical models for oligonucleotide structures in solution. Biopolymers *73*, 369–379.

Cheatham, T.E., III, and Kollman, P.A. (2000). Molecular dynamics simulation of nucleic acids. Annu. Rev. Phys. Chem. *51*, 435–471.

Cheatham, T.E., III, and Young, M.A. (2001). Molecular dynamics simulation of nucleic acids: successes, limitations, and promise. Biopolymers *56*, 232–256.

Cornell, W.D., Cieplak, P., Bayly, C.I., Gould, I.R., Merz, K.M., Ferguson, D.M., Spellmeyer, D.C., Fox, T., Caldwell, J.W., and Kollman, P.A. (1996). A second generation force field for the simulation of proteins, nucleic acids, and organic molecules. J. Am. Chem. Soc. *117*, 5179–5197.

Crothers, D.M., and Shakked, Z. (1999). DNA bending by adenine-thymine tracts. In Oxford Handbook of Nucleic Acid Structures, S. Neidle, ed. (London: Oxford University Press), pp. 455–470.

Dickerson, R.E. (1998). DNA bending: the prevalence of kinkiness and the virtues of normality. Nucleic Acids Res. *26*, 1906–1926.

Dixit, S.B., Pitici, F., and Beveridge, D.L. (2004). Structure and axis curvature in two $dA_6{\cdot}dT_6$ DNA oligonucleotides: comparison of molecular dynamics simulations with results from crystallography and NMR spectroscopy. Biopolymers *75*, 468–479.

Djuranovic, D., and Hartmann, B. (2003). Conformational characteristics and correlations in crystal structures of nucleic acid oligonucleotides: evidence for sub-states. J. Biomol. Struct. Dyn. *20*, 771–788.

Djuranovic, D., Oguey, C., and Hartmann, B. (2004). The role of DNA

structure and dynamics in the recognition of bovine papillomavirus E2 protein target sequences. J. Mol. Biol. *339*, 785–796.

Gabb, H.A., Lavery, R., and Prevost, C. (1995). Efficient conformational space sampling for nucleosides using internal coordinate Monte Carlo simulations and a modified furanose description. J. Comput. Chem. *16*, 667–680.

Gabb, H.A., Prevost, C., Bertucat, G., Robert, C.H., and Lavery, R. (1997). Collective-variable Monte Carlo simulations of DNA. J. Comput. Chem. *18*, 2001–2011.

Garvie, C.W., and Wolberger, C. (2001). Recognition of specific DNA sequences. Mol. Cell *8*, 937–946.

Gorin, A.A., Zhurkin, V.B., and Olson, W.K. (1995). B-DNA twisting correlates with base-pair morphology. J. Mol. Biol. *247*, 34–48.

Hegde, R.S. (2002). The papillomavirus E2 proteins: structure, function, and biology. Annu. Rev. Biophys. Biomol. Struct. *31*, 343–360.

Hegde, R.S., Grossman, S.R., Laimins, L.A., and Sigler, P.B. (1992). Crystal structure at 1.7 Å of the bovine papillomavirus-1 E2 DNA-binding domain bound to its DNA target. Nature *359*, 505–512.

Hines, C.S., Meghoo, C., Shetty, S., Biburger, M., Brenowitz, M., and Hegde, R.S. (1998). DNA structure and flexibility in the sequence-specific binding of papillomavirus E2 proteins. J. Mol. Biol. *276*, 809–818.

Hingerty, B.E., Ritchie, R.H., Ferrell, T.L., and Turner, J.E. (1985). Dielectric effects in biopolymers: the theory of ionic saturation revisited. Biopolymers *24*, 427–439.

Hizver, J., Rozenberg, H., Frolow, F., Rabinovich, D., and Shakked, Z. (2001). DNA bending by an adenine–thymine tract and its role in gene regulation. Proc. Natl. Acad. Sci. USA *98*, 8490–8495.

Kim, Y., Geiger, J.H., Hahn, S., and Sigler, P.B. (1993). Crystal structure of a yeast TBP/TATA-box complex. Nature *365*, 512–520.

Kim, S.S., Tam, J.K., Wang, A.F., and Hegde, R.S. (2000). The structural basis of DNA target discrimination by papillomavirus E2 proteins. J. Biol. Chem. *275*, 31245–31254.

Lavery, R., and Sklenar, H. (1988). The definition of generalized helicoidal parameters and of axis curvature for irregular nucleic acids. J. Biomol. Struct. Dyn. *6*, 63–91.

Lavery, R., and Sklenar, H. (1989). Defining the structure of irregular nucleic acids: conventions and principles. J. Biomol. Struct. Dyn. *6*, 655–667.

Lewis, M., Chang, G., Horton, N.C., Kercher, M.A., Pace, H.C., Schumacher, M.A., Brennan, R.G., and Lu, P. (1996). Crystal structure of the lactose operon repressor and its complexes with DNA and inducer. Science *271*, 1247–1254.

Li, T., Stark, M.R., Johnson, A.D., and Wolberger, C. (1995). Crystal structure of the MATa1/MAT α 2 homeodomain heterodimer bound to DNA. Science *270*, 262–269.

Luscombe, N.M., Laskowski, R.A., and Thornton, J.M. (2001). Amino acid-base interactions: a three-dimensional analysis of protein-DNA interactions at an atomic level. Nucleic Acids Res. *29*, 2860–2874.

Mazur, A.K., and Kamashev, D.E. (2002). Comparative bending dynamics in DNA with and without regularly repeated adenine tracts. Phys. Rev. E *66*, 011917.

McConnell, K.J., and Beveridge, D.L. (2000). DNA structure: what's in charge? J. Mol. Biol. *304*, 803–820.

McConnell, K.J., and Beveridge, D.L. (2001). Molecular dynamics simulations of B'-DNA: sequence effects on A-tract-induced bending and flexibility. J. Mol. Biol. *314*, 23–40.

Metropolis, N., Rosenbluth, A.W., Rosenbluth, M.N., Teller, A.H., and Teller, E. (1953). Equation of state calculations by fast computing machines. J. Chem. Phys. *21*, 1087–1092.

Olson, W.K., Gorin, A.A., Lu, X.J., Hock, L.M., and Zhurkin, V.B. (1998). DNA sequence-dependent deformability deduced from protein-DNA crystal complexes. Proc. Natl. Acad. Sci. USA *95*, 11163–11168.

Parkinson, G., Wilson, C., Gunasekera, A., Ebright, Y.W., Ebright, R.E., and Berman, H.M. (1996). Structure of the CAP-DNA complex at 2.5 angstroms resolution: a complete picture of the protein-DNA interface. J. Mol. Biol. *260*, 395–408.

Ponomarev, S.Y., Thayer, K.M., and Beveridge, D.L. (2004). Ion motions in molecular dynamics simulations on DNA. Proc. Natl. Acad. Sci. USA *101*, 14771–14775.

Rohs, R. (2002). Simulation of structure formation and ligand binding of nucleic acids in the space of collective and internal variables. PhD thesis, Freie Universität, Berlin, Germany (http://www.diss.fu-berlin.de/2003/3/).

Rohs, R., Etchebest, C., and Lavery, R. (1999). Unraveling proteins: a molecular mechanics study. Biophys. J. *76*, 2760–2768.

Rozenberg, H., Rabinovich, D., Frolow, F., Hegde, R.S., and Shakked, Z. (1998). Structural code for DNA recognition revealed in crystal structures of papillomavirus E2-DNA targets. Proc. Natl. Acad. Sci. USA *95*, 15194–15199.

Shatzky-Schwartz, M., Arbuckle, N.D., Eisenstein, M., Rabinovich, D., Bareket-Samish, A., Haran, T.E., Luisi, B.F., and Shakked, Z. (1997). X-ray and solution studies of DNA oligomers and implications for the structural basis of A-tract-dependent curvature. J. Mol. Biol. *267*, 595–623.

Sklenar, H., Wüstner, D., and Rohs, R. (2005). Using internal and collective variables in Monte Carlo simulations of nucleic acid structures: chain breakage/closure algorithm and associated Jacobians. J. Comput. Chem., in press.

Sprous, D., Young, M.A., and Beveridge, D.L. (1999). Molecular dynamics studies of axis bending in $d(G_5\text{-}(GA_4T_4C)_2\text{-}C_5)$ and $d(G_5\text{-}(GT_4A_4C)_2\text{-}C_5)$: effects of sequence polarity on DNA curvature. J. Mol. Biol. *285*, 1623–1632.

Stefl, R., Wu, H., Ravindranathan, S., Sklenar, V., and Feigon, J. (2004). DNA A-tract bending in three dimensions: solving the dA4T4 vs. dT4A4 conundrum. Proc. Natl. Acad. Sci. USA *101*, 1177–1182.

Stofer, E., and Lavery, R. (1994). Measuring the geometry of DNA grooves. Biopolymers *34*, 337–346.

Strahs, D., and Schlick, T. (2000). A-tract bending: insights into experimental structures by computational models. J. Mol. Biol. *301*, 643–663.

Varnai, P., and Zakrzewska, K. (2004). DNA and its counterions: a molecular dynamics study. Nucleic Acids Res. *32*, 4269–4280.

Winger, R.H., Liedl, K.R., Pichler, A., Hallbrucker, A., and Mayer, E. (1999). Helix morphology changes in B-DNA induced by spontaneous B_I-B_{II} substate interconversion. J. Biomol. Struct. Dyn. *17*, 223–235.

Young, M.A., and Beveridge, D.L. (1998). Molecular dynamics simulations of an oligonucleotide duplex with adenine tracts phased by a full helix turn. J. Mol. Biol. *281*, 675–687.

Zhang, Y.L., Xi, Z.Q., Hegde, R.S., Shakked, Z., and Crothers, D.M. (2004). Predicting indirect readout effects in protein-DNA interactions. Proc. Natl. Acad. Sci. USA *101*, 8337–8341.

Zhurkin, V.B., Ulyanov, N.B., Gorin, A.A., and Jernigan, R.L. (1991). Static and statistical bending of DNA evaluated by Monte Carlo simulations. Proc. Natl. Acad. Sci. USA *88*, 7046–7050.

Zimmerman, J.M., and Maher, L.J., III. (2003). Solution measurement of DNA curvature in papillomavirus E2 binding sites. Nucleic Acids Res. *31*, 5134–5139.